geosciences

MDPI

Article

Evidence of Seismic-Related Liquefaction Processes within the Volcanic Record of the Campi Flegrei Caldera (Italy)

Stefano Vitale [1,*], Jacopo Natale [1], Roberto Isaia [2], Francesco D'Assisi Tramparulo [3] and Sabatino Ciarcia [4]

[1] Dipartimento Scienze della Terra, dell'Ambiente e delle Risorse, Università di Napoli Federico II, Via Cupa Nuova Cintia 21, 80126 Napoli, Italy; jacopo.natale@unina.it
[2] Istituto Nazionale di Geofisica e Vulcanologia—Osservatorio Vesuviano, Via Diocleziano 328, 80124 Napoli, Italy; roberto.isaia@ingv.it
[3] Independent Researcher, 80100 Napoli, Italy; tramparulo.francesco83@gmail.com
[4] Dipartimento di Scienze e Tecnologie, Università del Sannio, via de Sanctis, 82100 Benevento, Italy; sabatino.ciarcia@unisannio.it
* Correspondence: stefano.vitale@unina.it

Abstract: We report the occurrence of several sand liquefaction structures, such as sand dikes, in the stratigraphic record of the Campi Flegrei volcano, located both inside and outside the caldera. Five sites were analyzed within the caldera and two outside. The grain size analysis of the sand fillings indicates that these deposits are very fine-to-coarse sands generally poorly sorted. All of the granulometry curves fall within the field of the liquefiable, loose sediments. Frequently, dikes are characterized by two fillings: a rim showing poorly sorted finer sands and a core with extremely poorly sorted coarser sediments. We suggest that seismic-related liquefaction processes triggered the injection of these sand dikes during unrest episodes in the last 15 kyr. In particular, the sand dikes located outside the caldera, characterized by larger thicknesses and lengths, mark an important extensional episode, probably associated with the caldera formation during the Neapolitan Yellow Tuff eruption at 15 ka. Furthermore, liquefaction structures within the caldera are related to the seismic activity, probably occurring during the Agnano–Monte Spina caldera formation and the volcano-tectonic ground deformation, predating Epoch 3b (4.3 ka) and the Monte Nuovo (1538 CE) eruptions. This study highlights that these seismic-related liquefaction structures are common within the volcanic record of the Campi Flegrei, suggesting that the sand source can be both the widespread marine succession underlying the Epoch 3 deposits in the caldera central sector and the primary ash layers extensively present in the volcanic record.

Keywords: sand dikes; sand liquefaction; Campi Felgrei; caldera; volcanoes

Citation: Vitale, S.; Natale, J.; Isaia, R.; Tramparulo, F.D.; Ciarcia, S. Evidence of Seismic-Related Liquefaction Processes within the Volcanic Record of the Campi Flegrei Caldera (Italy). *Geosciences* **2022**, *12*, 241. https://doi.org/10.3390/geosciences12060241

Academic Editors: Olivier Lacombe and Jesus Martinez-Frias

Received: 16 March 2022
Accepted: 6 June 2022
Published: 9 June 2022

1. Introduction

Seismic shaking can produce many effects on the ground; amongst others, one of the most spectacular is sand liquefaction, consisting of the fluidization of water-saturated sandy deposits and an injection into the host rock (e.g., [1]). This phenomenon can cause, in urbanized areas, severe damage to buildings and other facilities (e.g., [2,3] and references therein). Seismically induced liquefaction occurs when loose sandy sediments behave like a liquid if subjected to a seismic shock as a consequence of the abrupt increase of the pore-water pressure that nullifies the sediment's rigidity (e.g., [4–13]). However, sand is suitable to liquefy if it is water-saturated, and its granulometric curve lies in a specific grain size range [14]. Seismic-related liquefaction and soft-sediment deformation phenomena are common worldwide [12], especially in orogenic chains where earthquakes frequently occur [8,13]. In such environments, liquefaction processes usually occur starting from moderate seismic magnitudes (Ms $\geq$ 4.2; [8]). In volcanic environments, sand liquefaction is typically associated with tectonic earthquakes (e.g., [15,16]); however, in some cases, volcano-tectonic unrests can also produce sustained seismic activity

and are able to trigger liquefaction and soft-sediment deformation. In volcanic settings, earthquakes result from a large variety of processes, from hydrothermal system pressure variations [17], magma intrusion and migration, energetic volcanic eruptions, and volcano-tectonic and caldera collapses at different scales [18,19]. Volcanic unrests are characterized by several concurrent processes, including ground deformation and an increase in hydrothermal and seismic activity [20]. This is particularly true for the long-lived calderas, where several unrest episodes are recorded by a complex stratigraphic record hosting different generations of deformation structures. This is the case of the Campi Flegrei (CF), a 12 km-wide caldera whose structure was controlled by the caldera-forming eruptions of Campanian Ignimbrite and Neapolitan Yellow Tuff that occurred at 40 and 15 ka, respectively [21–23]. The subsequent volcano-tectonic activity was expressed by more than 70 monogenic eruptions, including the Plinian eruptions of Pomici Principali (12 ka) and Agnano–Monte Spina (4.55 ka) that formed two minor calderas [24]. These events produced different deformation structures, mainly represented by faults and fractures and characterized by different orientations and displacements that shaped the morphology of the caldera floor. However, particular kinds of deformation structures, such as sand dikes, are reported in the CF [19]. These structures have been interpreted as related to paleoliquefaction episodes that triggered the formation of sand injections along the fractures and faults [19]. This study aims to provide evidence of such structures within the volcanic record of the CF and mark that sand liquefaction is not a rare process within the history of the CF and, hence, it has to be considered as a further potential hazard in the risk assessment of future unrest crises.

2. Geological Setting

The Tyrrhenian margin of the southern Apennines in the Campania region [25,26] hosts the Campi Flegrei caldera (CFc; [19,27,28]), Somma-Vesuvio (e.g., [29,30]), and Ischia Island (e.g., [31]), three active volcanoes surrounding the urban area of Naples. The onset of volcanism at the CFc is dated back to 80-100 ka [32,33], with scattered explosive and subordinately effusive volcanism across the Neapolitan area (e.g., [21,34]). Two large ignimbrite eruptions mark the evolution of this volcanic field, namely the Campanian Ignimbrite at 40 ka (CI; [23,35]) and the Neapolitan Yellow Tuff at 15 ka (NYT; [22]). These eruptions created a nested caldera that first formed with the CI eruption, subsequently reactivated by the NYT [36,37]. These eruptions dispersed a large amount of ash toward the southern Apennines and beyond, representing exceptional tephrostratigraphic markers (e.g., [38]). Very intense volcanism followed the NYT eruption, whose location was mostly controlled by the position of the caldera rims and preexisting structures [37,39–41]. The volcanic evolution of the last 15 kyr is composed of three periods of activity, called Epochs [24,42,43], and was interrupted by centuries-to-millennia quiescence periods. The volcanic activity in Epochs 1, 2, and 3 occurred at 14.9–10.6, 9.6–9.1, and 5.5–3.7 ka, respectively ([41] and references therein). Epoch 3 was further subdivided into Epoch 3a and 3b due to a significant pause and ground deformation following the Agnano–Monte Spina eruption (AMS, 4.55 ka; [27,44]). Remarkably, volcanism was coupled with significant ground deformation, which appears to be confined within the caldera rim [45]. The volcano-tectonic evolution resulted in a continuous interplay between volcanism and marine sedimentation. The record of the ground deformation is exceptionally well-recorded onshore by the marine-transitional La Starza Unit ([28] and references therein) and offshore, where over one-third of the caldera is submerged beneath the present-day Pozzuoli Gulf [46–48]. These successions recorded several phases of marine ingressions and regressions related to sea-level rise [49] and ground deformation [28,47]. After millennia of repose, the CFc produced its last eruption in historical times in 1538 CE, with the formation of the volcano of Monte Nuovo [50]. This eruption was preceded and accompanied by earthquakes that caused severe damage to the buildings, as reported by the historical chronicles [50]. Since 1950,

the CFc activity has been characterized by a net uplift of ~380 cm centred at the town of Pozzuoli [51] and intense seismic and hydrothermal activity, especially in the Solfatara [52] and Pisciarelli areas [53,54]. More than 16,000 recorded earthquakes occurred in the 1982–1984 crisis, with a maximum magnitude of 4.2 Ml [39]. Subsequently, the seismic activity ended synchronously with a general caldera ground subsidence until 2005, when the uplift renewed. The ongoing unrest generally shows lesser seismicity than the 1982–1984 activity, with a maximum magnitude of 3.6 Md in 2022 [51].

3. Materials and Methods

We report the occurrence of sand dikes in different outcrops, both in the central sector of the CFc (sites 1 to 5; Figure 1) and outside (sites 6 and 7; Figure 1). We collected several samples of sands within the analyzed dikes to carry out a grain-size analysis. We used the sieve analysis to estimate the cumulative curves of passing sediment percentage. In order to evaluate the median grain size and sorting and the uniformity coefficients, we defined the grain sizes D_{10}, D_{16}, D_{50}, D_{60}, and D_{84} as corresponding to the 10-16-50-60-84% of passing sediments. Subsequently, we calculated the median diameter corresponding to the grain size D_{50}, the sorting coefficient Sc estimated as $(D_{84}/D_{16})^{1/2}$ [55], and, finally, the uniformity coefficient Uc calculated as D_{10}/D_{60}. Sands are generally formed by white to grey ash with abundant sanidine and biotite crystal fragments. The coarser sands in site 7 (the Zaccaria quarry) include subangular fragments of obsidian, dense glass shards, pumice, and lavas. In site 1 (COPIN area), sponge spicules are present in the sands.

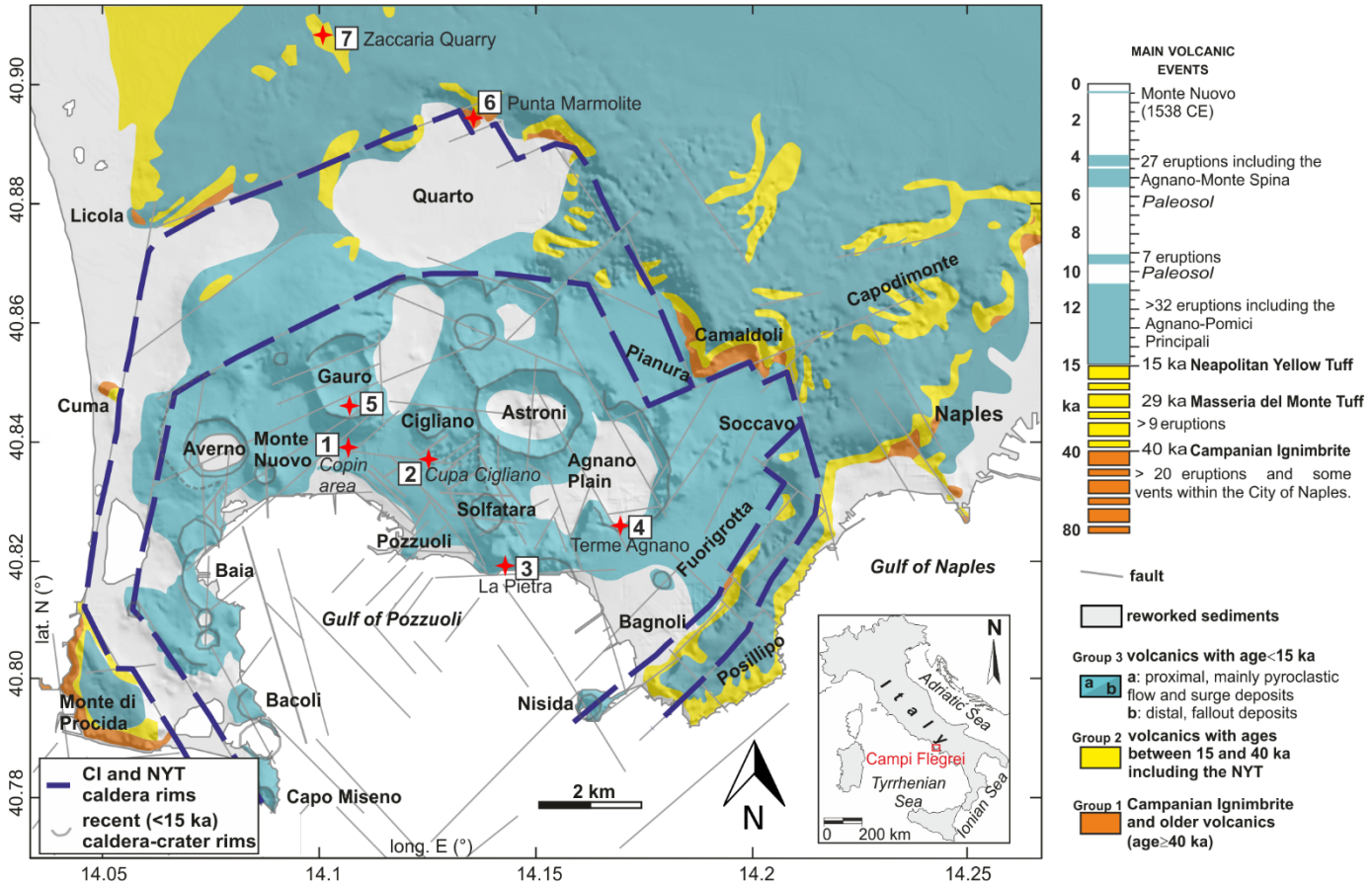

Figure 1. Geological sketch of the Campi Flegrei shows the sites of the studied paleo-liquefaction structures (modified after [19]).

4. Results

4.1. Grain Size Analysis

The grain size curves are shown in Figure 2a. Most profiles have an upward convex shape; others show linear or downward convex curves. All the curves indicate that these deposits are characterized by dominant granular particles in the range of sands. Figure 2b shows the scatter plot of median grain size, Φ ($\log_2(D_{50})$) vs. the sorting coefficient, Sc. According to the classification of [56], 61% of median grain sizes fall in the range of very fine to fine sands. The sorting coefficient is classified according to [55]. The samples are dominantly very poorly sorted (71%), and only some COPIN (site 1) samples are poorly sorted (13%; Figure 2b). In particular, we observed that overall, the sands sampled in the dike rims are finer and relatively more sorted compared to the cores. To investigate if the grain size curves fall in the liquefaction probability field [14], we divided the grain-size curve according to their uniformity coefficient; the first group is characterized by a Uc < 3.5 (Figure 2c) and the second by a Uc > 3.5 (Figure 2d). The majority of the grain size curves have a Uc > 3.5, and only five samples of COPIN and one of the Gauro (site 5) show a Uc < 3.5.

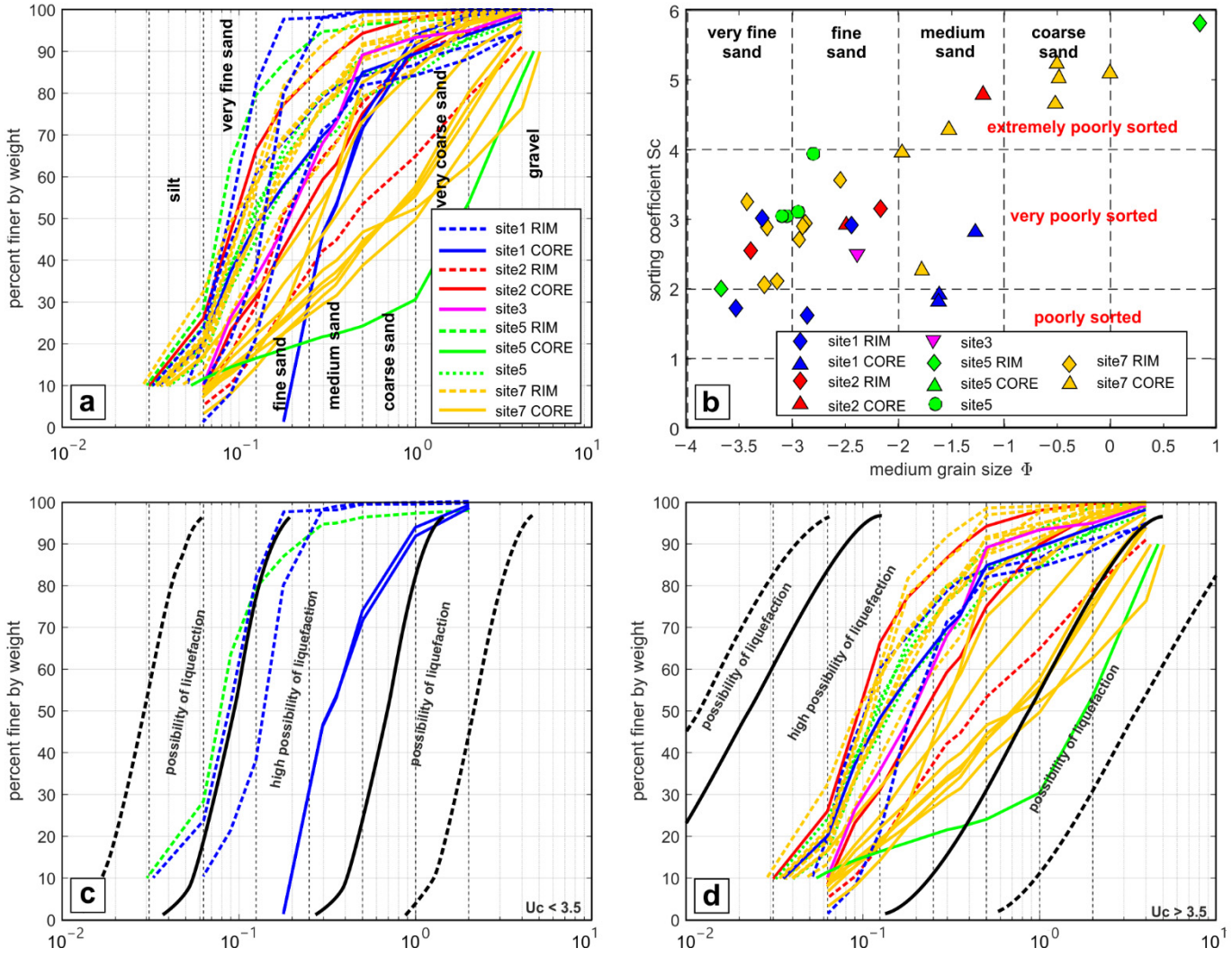

Figure 2. (**a**) Cumulative diagram of the grain size of the collected samples. (**b**) Scatter plot of Cs vs. D50. Cumulative diagram of the grain size of the collected samples with a Uc < 3.5 (**c**) and a Uc > 3.5 (**d**), modified after [14].

4.2. Structures

The first analyzed outcrop is located in the COPIN area (site 1), between the Gauro volcano to the North and the coast of Pozzuoli to the South (Figure 1). Here, the sedimentary succession is characterized by the La Starza marine-transitional deposits (12–5.86 ka; [28]), covered by the continental volcanic sequences of Epoch 3 [28]. The succession hosts several deformation structures [19], including faults, sand dikes, sand injections, and sand volcanoes (Figure 3). A major E-W trending dike is present (Figure 3a) with a thickness of ~16 cm within the paleosol overlying the AMS deposits (4.55 ka). It is characterized by a medium sand core bounded by two thin fine sand rims. Other smaller dikes are present running along a ~E-W direction (Figure 3b). Some thick dikes are dismembered within the paleosol (Figure 3c). The main dike has fed a sand volcano covering the paleosol (Figure 3d), defined by a 50 cm height and gently dipping flanks. This structure is covered by the AVS deposits (4.28 ka). A zoomed section of the volcano flank shows a layered upward coarsening deposit (Figure 3e). During the excavation of the gallery joining the Gauro area to the Pozzuoli harbour, several sand dikes and injections were found in the La Starza succession [19]. In particular, sand injections in the footwall of normal faults are common features (Figure 3f), as well as sand dikes showing normal offsets (hybrid faults) (Figure 3g).

The second site is located to the South of the Cigliano volcano (Cupa Cigliano, site 2 in Figure 1). Here, the Astroni succession (4.2 ka; [57]) is made of alternations of thin-bedded ash layers and stratified pumice lapilli beds. These deposits are cross-cut by an ~E-W normal fault zone dipping to the South. It includes an array of normal faults forming a dip relay zone [58] that displaces the tephra layers up to 1.5 m.

A 10 cm thick sand dike is located in its footwall with an N-S direction (Figure 4a). The dike is characterized by medium sand showing some anastomosing thin internal layers of fine sand within a medium sand matrix embedding pumice lapilli (Figure 4c). In the Terme di Agnano (site 3 in Figure 1), the Costa San Domenico volcanic succession (~9.5 ka; CSD; Epoch 2; [43]) is exposed along a road cut. It is made of thinly stratified ash and pumice lapilli layers, hosting sand dikes thinning upward (Figure 4c) and sand injections in the footwall of the ~E-W conjugate normal faults (Figure 4d).

The area around the La Pietra (site 4 in Figure 1) is defined by the tuff lithosome of La Pietra (14 ka) covered by the La Starza Unit and the Epoch 3a volcanics, which are, in turn, composed of alternate accretionary lapilli-bearing ash layers and paleosols. Here, the deposits host several faults showing normal and reverse kinematics characterized by an NW-SE to E-W directions. Several sand injections are associated with these faults and are commonly hydrothermally altered (Figure 4a).

Site 5 (Figure 1) is located along the inner southern slope of the Gauro tuff cone (14 ka). The tuff is covered by primary and reworked pyroclastic products of the Epoch 3 eruptions, including Cigliano (CIG, 5.25 ka), Monte Sant'Angelo (MSA, 4.9 ka), Paleoastroni 2 (PA2, 4.7 ka), and AMS (4.55 ka) tephra. These products are made of ash and pumice lapilli layers, interbedded to paleosol and humified layers. The pyroclastic succession hosts different sand dikes (Figure 5b–g). The larger one (Figure 5b) shows a peculiar ramp-flat geometry, defined by two ramps bounding a flat-lying that is parallel to the volcanic layering. Another feature that characterizes this structure is the disarticulation of several parts (Figure 5c). A minor E-W-directed Neptunian sand dike is associated with a normal fault with centimetric displacement within the MSA and PA2 tephra layers (Figure 5d). Another major dike (Figure 5e) cross-cuts the CIG and MSA tephra, with a thickness of ~12 cm. It is composed of different sand injections with downward convex laminations (Figure 4f); the core is defined by coarser sands than the rim, showing finer sands and, locally, tiny fingers (Figure 5g). The Punta Marmolite lava dome (site 6 in Figure 1) is located along the northern caldera rim, North of the Quarto Plain. Here, a pre-CI succession is exposed and is constituted by lava and breccia deposits, hosting some thin sand dikes (Figure 6a).

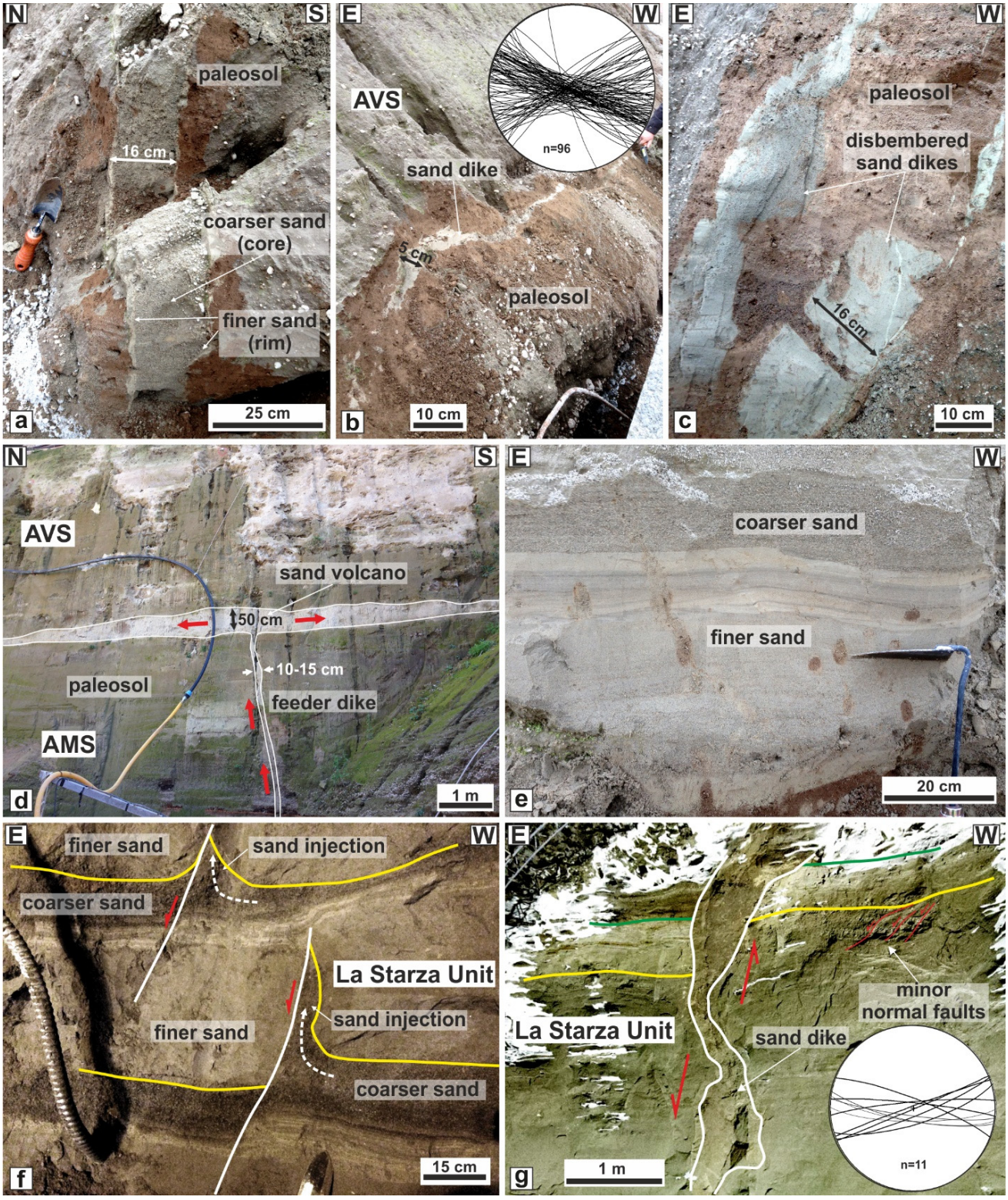

Figure 3. COPIN area (site 1). (**a**,**b**) Sand dike within the paleosol covering the AMS deposits and stereographic projection of dike boundaries. (**c**) Dismembered sand dike. (**d**) Sand volcano with feeding dike. (**e**) A section of the sand volcano flank. (**f**) Sand injections in the footwall of normal faults. (**g**) Hybrid normal fault with sand injection and stereographic projection of fault planes.

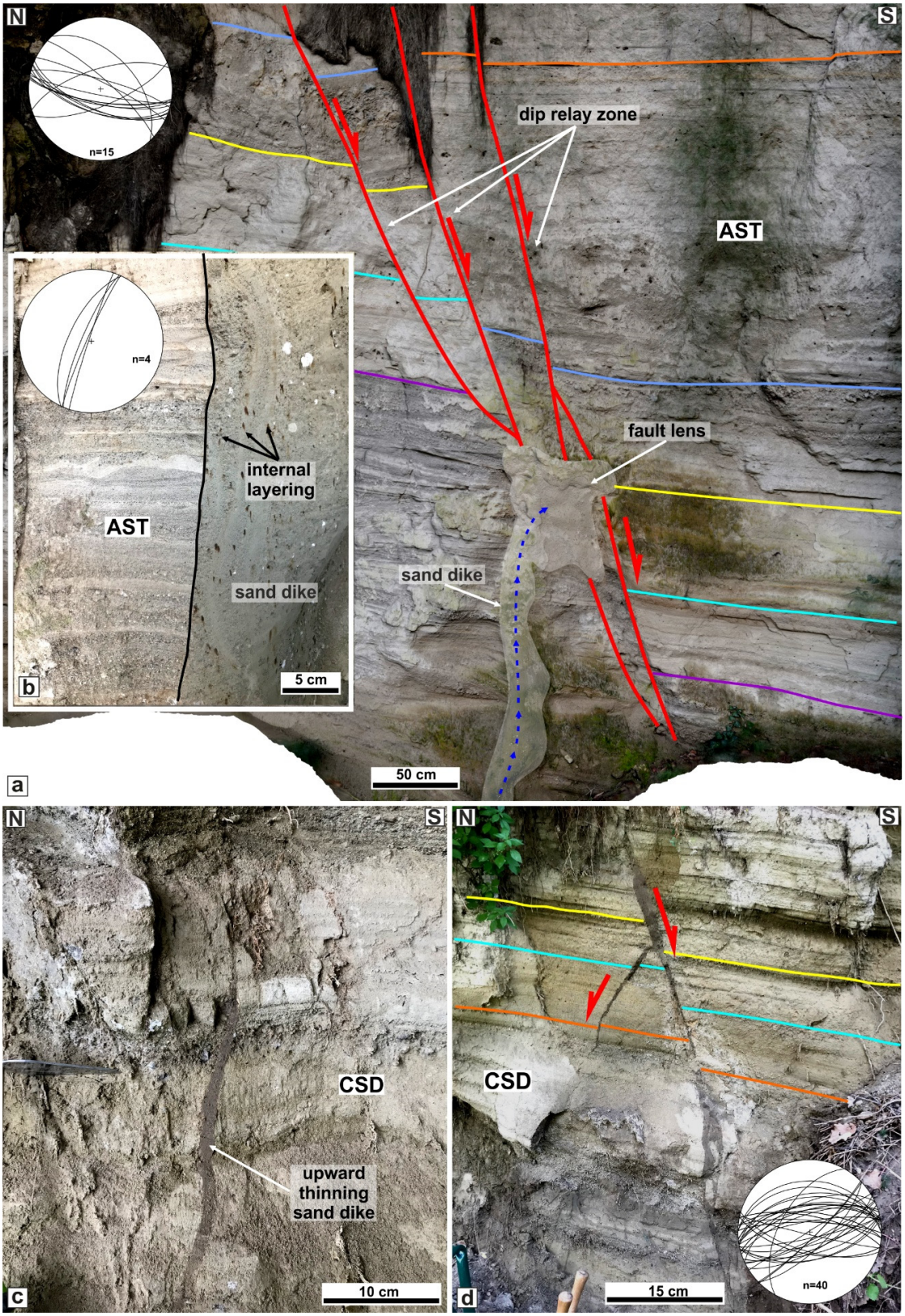

Figure 4. Cupa Cigliano (site 2): (**a**) ~E-W normal fault cross-cutting Astroni (AST) tephra and the sand dike, and stereographic projection of fault planes; (**b**) view along the strike of the sand dike; (**c**) Terme Agnano (site 3): sand dike thinning upward within the Costa San Domenico (CSD) tephra; (**d**) EW conjugate normal faults with associated sand injections in the footwall, and stereographic projection of fault planes.

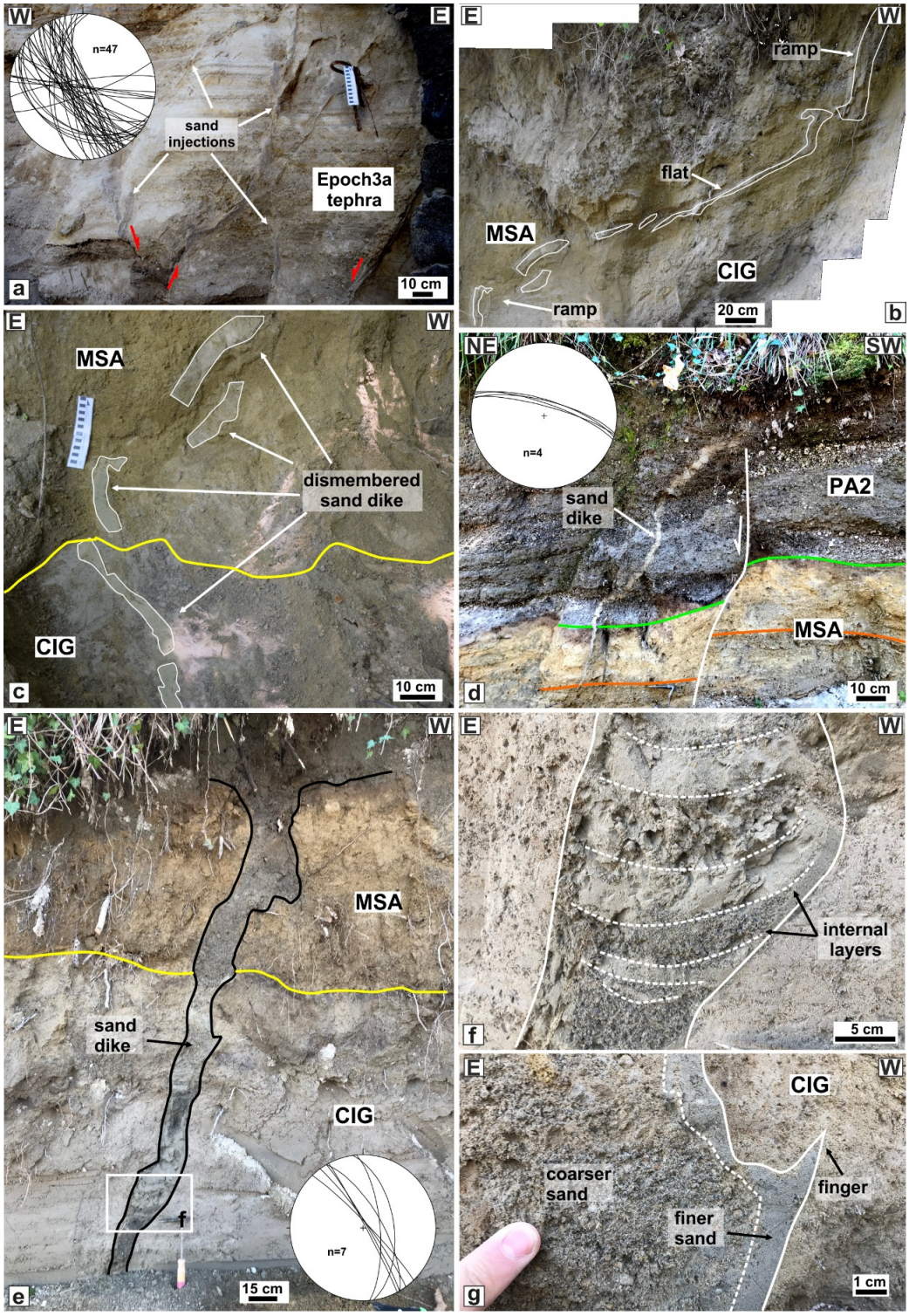

Figure 5. La Pietra (site 4): (**a**) sand injections associated with several faults within Agnano 1-2 tephra and stereographic projection of fault planes. Gauro volcano (site 5): (**b**) panoramic view of a ramp-flat sand dike within Cigliano (CIG) tephra; (**c**) particular of the dismembered dike; (**d**) Neptunian dike and normal faults within Paleoastroni2 (PA2) and Monte Sant'Angelo (MSA) tephra, and stereographic projection of dike boundaries; (**e**) sand dike with dewatering structures within MSA and Cigliano tephra, and stereographic projection of dike boundaries; (**f**) particular of the dike showing the downward convex lamination; (**g**) particular of the dike showing the coarser core and finer rim with a small finger.

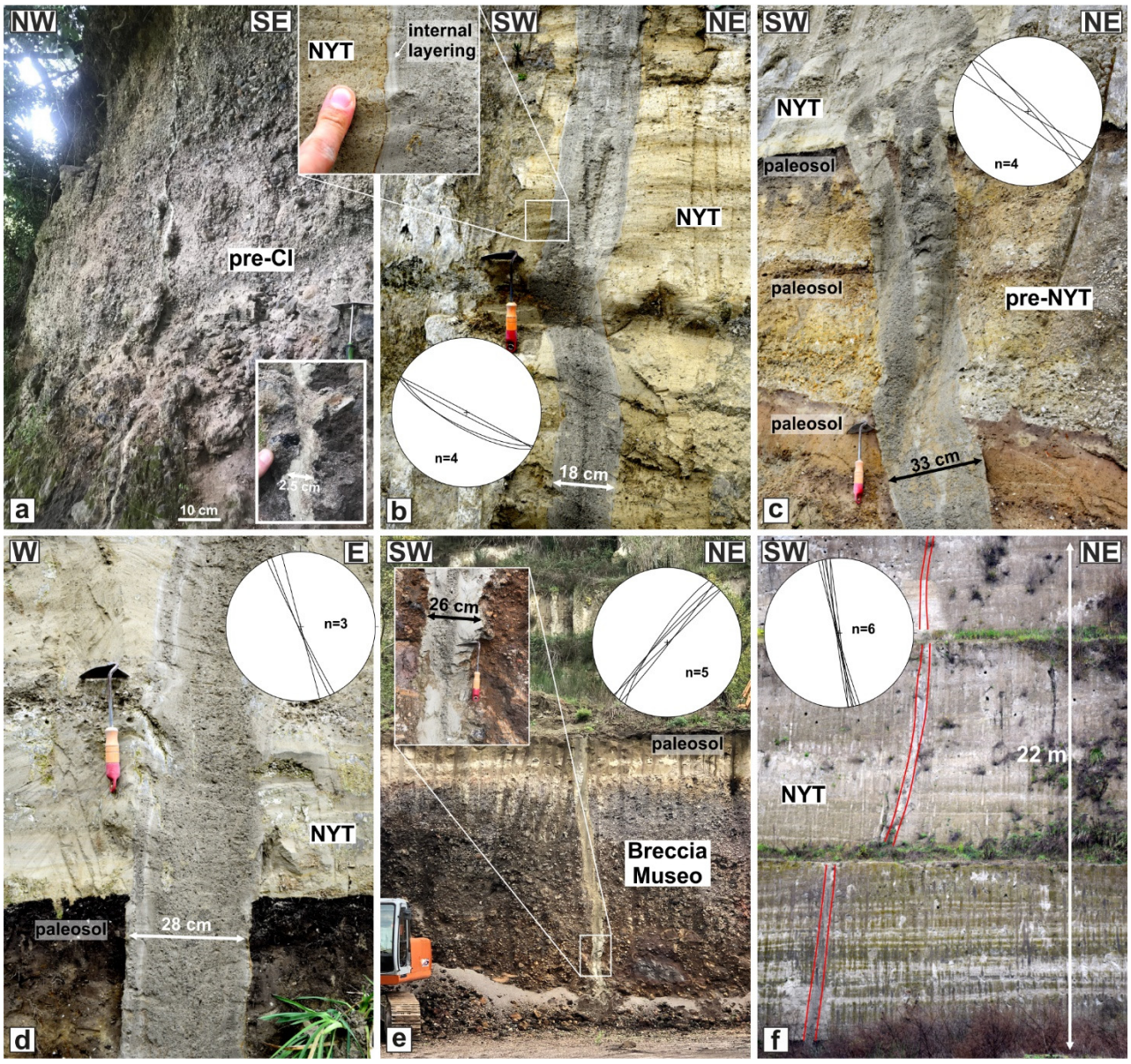

Figure 6. Punta Marmolite (site 6): (**a**) sand dike within the breccia deposit of the Punta Marmolite lava dome. Zaccaria quarry (site 7): (**b**–**d**) sand dikes within the pre-NYT and NYT tephra layers; (**e**) sand dike cross-cutting the Breccia Museo Unit of the Campanian Ignimbrite deposit; (**f**) sand dike hosted in the NYT with a length larger than 22 m. Stereographic projections of dike boundaries are shown in (**b**–**f**).

Finally, site 7 is located outside the CFc, within a pozzolana quarry (the Zaccaria quarry; Figure 1). The area is characterized by a pyroclastic succession formed from the bottom to the top by the Breccia Museo Unit of CI, several pre-NYT tephra and paleosol, and the unconsolidated pyroclastic deposit of NYT (pozzolana). Here, several major sand dikes are present in a 0.15 km^2 area, of which eight were measured and sampled (Figure 6b–f). The largest sand dikes are characterized by a thickness ranging between 18 and 33 cm. In some cases, dikes are formed by the coalescence of two dikes (Figure 6c). Usually, the contact between the dikes and the host rock is sharp (see the inset of Figure 6b). All the dikes are formed by two sand sediments, a rim of a few centimetres formed by finer sands, and a core with a coarser grain size (Figure 6b–e). They are very steep (the mean is 85° of the dip) with an orientation of NW-SE, NE-SW, N-S, and E-W, and they reach lengths exceeding 22 m (Figure 6f).

5. Discussion

We found several sites where sand dikes are exposed; they are mostly located in the central part of the CFc, whereas others are along the CI rim and outside the caldera. The first group (sites 1–5) includes sand dikes hosted within the volcanic successions younger than NYT (15 ka), whereas the second group (sites 6–7) encompasses dikes within the NYT or older tephra. Most of the dikes are associated with faults, suggesting a close relationship between the origin of these structures and the different faulting episodes that have characterized the CFc's evolution in the last 15 kyr [19]. One of the most outstanding outcrops is located in the COPIN area (Figure 1). Here, several structures, such as dikes, sand volcanoes, and faults, occur (Figure 3). The presence of a sand volcano fed by a sub-vertical dike is evidence of liquefaction processes that allow liquified sediments to migrate upward (e.g., [59]). The main dike (Figure 3a) shows two different sand grain sizes, finer along the contact with the host rock and coarser in the central part. Such different granulometry is also observed in the section of the sand volcano flanks (Figure 3e), with the finer one located in the lower part. Such features suggest two steps of emplacement during liquefaction processes, with the former characterized by finer sands and the latter involving coarser sands. Soft-sediment deformation is observed as sand injections in the footwall of normal faults (Figure 3f) and sand dikes featuring normal displacement (Figure 3g). According to [19], the sediments forming the sand volcanoes and the dike fillings are the marine sands of the La Starza Unit. The presence of sponge spicules within the dike's fillings corroborates this interpretation.

Due to the evidence that sand dikes and volcanoes are hosted within the AMS tephra (4.55 ka) and are sealed by AVS (4.28 ka) deposits, [19] associated the emplacement of these structures with an unrest episode that occurred before the eruption of the AVS. Furthermore, such structures are coupled with faults showing the same cross-cutting relationships with the volcanic record [19]. Following the Plinian eruption of AMS, which was associated with the formation of a minor caldera [60], the CF was affected by subsidence witnessed by the marine ingression and sedimentation of the marine/transitional deposit of the Pozzuoli Unit [44]. Offshore, this unit frequently appears as massive gravity flow deposits embedded between the AMS and AVS (Figure 7a), suggesting that a significant instability of the coastal sector characterized this unrest event. Such features indicate that the paleoliquefaction process was triggered by earthquakes associated with the unrest predating the start of Epoch 3b. In addition, sand dikes and related normal faults mark a ground extension that can be imaged as associated with a lateral spreading. The latter process is frequently coupled with liquefaction and gravitational instability along coastal environments [61,62].

The sand dike located in site 2 is hosted in the AST succession (Figure 3a). It is genetically related to the normal fault zone; in fact, it is orthogonal to the fault planes and intrudes within the fault zone lens (Figure 3a), probably due to the more intense fracturing of this sediment volume. The sand injection does not continue upward in the hanging wall, suggesting it migrated horizontally following the E-W-directed relay zone. Therefore, the liquefaction episode that caused the sand injection is subsequent to the faulting. The E-W faults are widespread in the whole central sector of the CF caldera [37,54] and are thought to be associated with the ground deformation of the Epoch 3b and the one the last eruption of Monte Nuovo at 1538 CE. It follows that the sand injection probably occurred triggered by a liquefaction process associated with the intense seismic activity anticipating the eruption [50]. The sand injections of site 3 (Figure 1) occur as single dikes with a tip tapering upward (Figure 3c) or as injections in the footwall of conjugate normal faults (Figure 3d) that clearly indicate an upward flow. A similar interpretation can be proposed for the dikes in the La Pietra outcrop (site 4), where sand injections are associated with faulting (Figure 4a). These structures are located in the hanging wall of a major normal fault that lowered the Epoch 3's successions with respect to the La Pietra lithosome (14 ka; [42]) toward the Agnano caldera, located to the North.

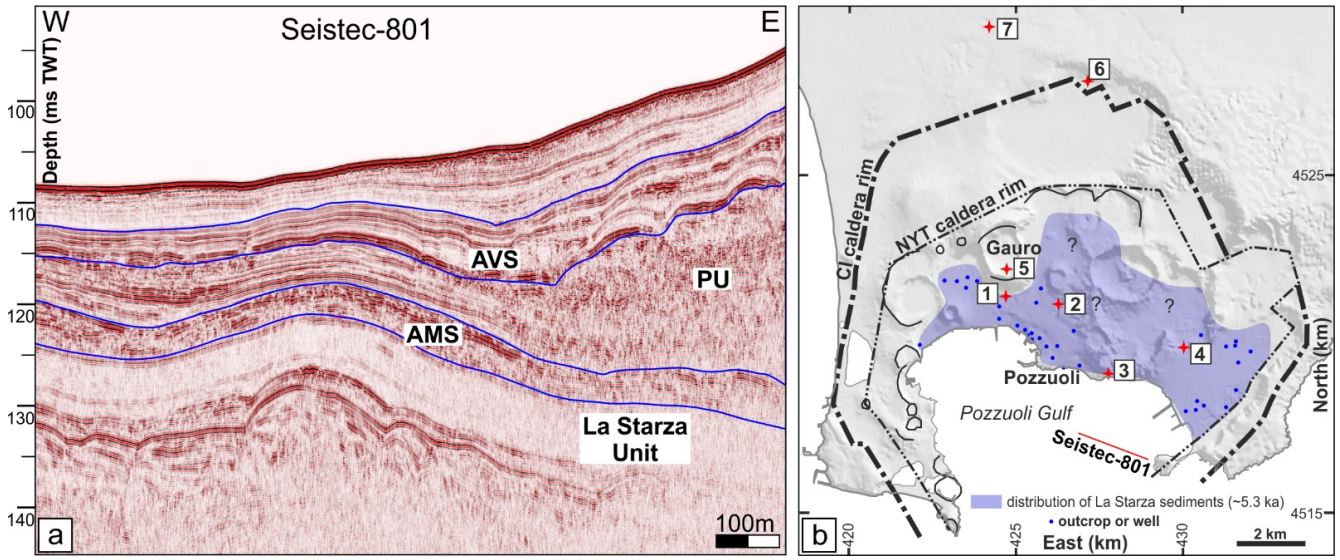

Figure 7. (**a**) Interpreted seismic profile within the Pozzuoli Gulf (after [47] modified). (**b**) Reconstruction of the La Starza sediment distribution (after [19] modified). AMS: Agnano–Monte Spina; PU: Pozzuoli Unit; AVS: Averno-Solfatara.

For sites 2–4, located within the CF caldera, it is reasonable to assume that the injected sands come from the marine/transitional La Starza sediments located just under the Epoch 3 deposits along the coast [28] and below the Epoch 2 inland [24], such as is indicated by the map of the spatial distribution (Figure 7b). However, we cannot exclude that the liquefied sands for these sites may come from volcanic ash layers because they are very poorly sorted sands (Figure 6b), a feature very common to volcanic deposits [63]. We can hypothesize that these structures, located along the rim of the Agnano Plain, have formed during the AMS eruption that formed this minor caldera.

Dikes observed in the Gauro volcano are hosted in the Epoch 3 deposits covering the volcanic edifice. The main dike (Figure 5b) shows a ramp-flat geometry, indicating that the liquefied sand came from below with a liquid pressure capable of creating a flat-lying fracture. The entire dike shows evidence of dismembering, suggesting that the deformation episode triggered a general ground instability, also marked by Neptunian dikes and minor normal faults (Figure 5d). In some cases (Figure 5e), the dike shows downward convex layers of alternating finer and coarser sands (Figure 5f), suggesting a possible later outflow of the sands after the injection (dewatering process, [64]). Because the outcrop is located at more than 300 m a.s.l., and the Gauro Tuff is several hundred meters thick, we can rule out a deep provenance of liquefied sands; instead, we argue that the liquefaction process affected water-saturated ash layers in surficial and/or perched aquifers.

Dikes located outside the CF caldera (sites 6 and 7) are hosted in a pre-CI deposit (Punta Marmolite) and within the CI and NYT (Zaccaria quarry). In the first site, the thickness is of few centimetres, but in the quarry, these structures show thicknesses of several tens of centimetres (up to 33 cm). Two sand fillings characterize all the dikes; the rims are defined by very fine to fine sands, whereas the cores are by medium to coarse sands (Figures 2b and 6b). The rim sands are very poorly sorted, and the core sands are generally extremely poorly sorted (Figure 2b). Such structures, showing a different grain size along the rim and core, are very similar to the dikes of site 1, and, like the latter structures, the Zaccaria quarry dikes can be interpreted as related to a similar process defined by seismic-related sand liquefaction with two injection steps, the former of finer sands and the latter of coarser sands. The large dike thicknesses and the widespread occurrence suggest that they were associated with a relevant extensional event. The lack of normal faults and a dike-parallel slip indicates that the process was characterized only by horizontal movements, such as lateral spreading. The length of these structures is

at least 30 m, indicating that the source of the liquefied sands is located at depth. The granulometry and sorting features of the dike sands, and the occurrence of obsidian within the coarser deposits, indicate that they probably originated from coarse volcanic ash layers located within the Breccia Museo Unit. We suggest that the trigger event that produced the liquefaction process of the dikes could be related to the NYT caldera formation or, less likely, to a regional tectonic seismic activity. In the former scenario, the last phases of the eruption and caldera-formation produced a radial extension outside the caldera and intense seismic activity that caused lateral spreading, sand liquefaction, and the upward migration of liquefied sands along fissures, randomly oriented.

The frequent occurrence of dikes formed by sands with two different grain sizes, finer along the rim and coarser in the core, can be associated with the grain size segregation phenomenon during the liquefaction process [65]. Segregation may occur both within the source layer and the dike itself [66,67], with the finer sediments moving and forming an infiltration layer and being injected upward, followed by the coarser sediments.

The widespread occurrence of structures associated with seismic-related liquefaction in the CF volcano indicates that this process is common during unrest periods. The structures located outside the caldera probably testify to volcano-tectonic events associated with the caldera formation, whereas the dikes located inside the CF caldera are related to minor deformation episodes, such as the unrest periods related to the Agnano Monte Spina eruption and the caldera formation (4.55 ka), or the seismo-volcanic unrest predating the eruptions of Epoch 3b (4.3 ka) and Monte Nuovo (1538 CE). Such evidence advises considering the seismic-related liquefaction as a process that can occur during volcano-tectonic unrests, taking into account, also, that the liquefiable sands can be not only the marine deposits of the La Starza succession located in the coastal/central caldera area but also the ash layers extensively occurring in the volcanic record within and outside the caldera.

6. Conclusions

The active volcano of Campi Flegrei hosts several sand dikes characterized by thicknesses ranging from a few to tens of centimetres, frequently associated with normal faults. These structures show fillings of sands, generally poorly sorted and with fine grain sizes. We associated these structures with a liquefaction process triggered by seismic activity. The grain size analysis indicates that the sand fillings fall within the field of potentially liquefiable sediments. We analyzed different outcrops, including sites within and outside the caldera. In the first case, we suggest that these structures are linked to unrest episodes occurring during Epoch 3 and in historical times. In particular, stratigraphic and structural evidence indicates that the sand dikes in the COPIN area are related to the unrest episode predating Epoch 3b, following a subsidence period marked by marine ingression and the deposition of the Pozzuoli Unit (4.4 ka). The deformation event is evidenced by the normal faults coupled with the sand dikes and the gravity flow of Pozzuoli Unit deposits along the seacoast in the Pozzuoli Gulf. Other sand dikes cross-cutting the Epoch 2 and 3a deposits can be related to the ground deformation following the Agnano–Monte Spina caldera formation (4.55 ka). Finally, sand dikes hosted in the pre-CI, CI, and NYT deposits testify to an important deformation event that could have occurred during the NYT caldera formation (15 ka). This deformation was dominantly expressed by tensile fractures filled with liquefied sands, suggesting a lateral spreading ground deformation for this area. Several dikes are characterized by internal sand layering with finer rims and coarser cores. We interpret this feature as a result of the grain size segregation phenomenon occurring during the liquefaction process. Finally, we emphasize that sand liquefaction is a common process within the volcano-tectonic evolution of the CFc, and, as such, it has to be considered as a further hazard during seismo-volcanic unrests.

Author Contributions: Conceptualization, S.V. and J.N.; methodology, S.V. and J.N.; software, S.V.; validation, S.V. and J.N.; formal analysis, S.V. and J.N.; investigation, S.V., J.N., R.I., F.D.T. and S.C.; resources, S.V., J.N. and R.I.; data curation, S.V., J.N., and S.C.; writing—original draft preparation, S.V., J.N. and S.C.; writing—review and editing, S.V., J.N., R.I., F.D.T. and S.C.; visualization, S.V. and J.N.; supervision, S.V. All authors have read and agreed to the published version of the manuscript.

Funding: This research received no external funding.

Data Availability Statement: Data are available at: https://osf.io/2s5wj/?view_only=0762df73ff4049d1a7dc7a46e263b174 (accessed on 1 June 2022).

Acknowledgments: We thank the owner and the workers of Zaccaria quarry for granting us access to the site and for the support and discussion during the field survey.

Conflicts of Interest: The authors declare no conflict of interest.

References

1. Ishihara, K. Liquefaction and Flow Failure during Earthquake. *Géotechnique* **1993**, *43*, 351–415. [CrossRef]
2. Huang, Y.; Yu, M. Review of soil liquefaction characteristics during major earthquakes of the twenty-first century. *Nat. Hazards* **2013**, *65*, 2375–2384. [CrossRef]
3. Kuribayashi, E.; Tatsuoka, F. Brief review of liquefaction during earthquakes in Japan. *Soils. Found* **1977**, *15*, 81–92. [CrossRef]
4. Allen, J.R.L. *Sedimentary Structures: Their Character and Physical Basis*; Elsevier: New York, NY, USA, 1982; Volume II.
5. Obermeier, S. Use of liquefaction-induced features for paleoseismic analysis—An overview of how seismic liquefaction features can be distinguished from other features and how their regional distribution and properties of source sediment can be used to infer the location and strength of Holocene paleo-earthquakes. *Eng. Geol.* **1996**, *44*, 1–76. [CrossRef]
6. Owen, G. Experimental soft-sediment deformation: Structures formed by the liquefaction of unconsolidated sands and some ancient examples. *Sedimentology* **1996**, *43*, 279–293. [CrossRef]
7. Tuttle, M.; Barstow, N. Liquefaction-related ground failure: A case study in the New Madrid seismic zone, central United States. *Bull. Seismol. Soc. Am.* **1996**, *86*, 636–645.
8. Galli, P. New empirical relationships between magnitude and distance for Liquefaction. *Tectonophysics* **2000**, *324*, 169–187. [CrossRef]
9. Montenat, C.; Barrier, P.; Ott d'Estevou, P.; Hibsch, C. Seismites: An attempt at critical analysis and classification. *Sediment. Geol.* **2007**, *196*, 5–30. [CrossRef]
10. Wang, C.Y. Liquefaction beyond the near field. *Seismol. Res. Lett.* **2007**, *78*, 512–517. [CrossRef]
11. Caputo, R.; Poli, M.E.; Minarelli, L.; Rapti, D.; Sboras, S.; Stefani, M.; Zanferrari, A. Palaeoseismological evidence for the 1570 Ferrara earthquake, Italy. *Tectonics* **2016**, *35*, 1423–1445. [CrossRef]
12. Tuttle, M.P.; Villamor, P.; Almond, P.; Bastin, S.; GionaBucci, M.; Langdridge, R.; Clark, K.; Hardwick, C. Liquefaction induced by the 2010–2011 Canterbury, New Zealand, Eartquake Sequence and Lessons Learned for the Study of Paleoliquefaction features. *Seismol. Res. Lett.* **2017**, *88*, 1403–1414. [CrossRef]
13. Cavallaro, A.; Capilleri, P.P.; Grasso, S. Site Characterization by Dynamic In Situ and Laboratory Tests for Liquefaction Potential Evaluation during Emilia Romagna Earthquake. *Geosciences* **2018**, *8*, 242. [CrossRef]
14. Lai, S.; Tsuchida, H.; Koizumi, K. A new criterion for assessing liquefaction potential using grain size accumulation curve and N-value. *Rep. Port Harb. Res. Inst.* **1986**, *25*, 125–234.
15. Kameda, J.; Kamiya, H.; Masumoto, H.; Morisaki, T.; Hiratsuka, T.; Inaoi, C. Fluidized landslides triggered by the liquefaction of subsurface volcanic deposits during the 2018 Iburi–Tobu earthquake, Hokkaido. *Sci. Rep.* **2019**, *9*, 13119. [CrossRef]
16. Ogo, K.; Hazarika, H.; Kokusho, T.; Matsumoto, D.; Ishibashi, S.; Sumartini, W.O. Analysis of liquefaction of volcanic soil during the 2016 Kumamoto Earthquake based on boring data. *Lowl. Technol. Int.* **2018**, *19*, 245–250.
17. McNutt, S.R. Seismic Monitoring and Eruption Forecasting of Volcanoes: A Review of the State-of-the-Art and Case Histories. In *Monitoring and Mitigation of Volcano Hazards*; Scarpa, R., Tilling, R.I., Eds.; Springer: Berlin/Heidelberg, Germany, 1996; pp. 99–146. [CrossRef]
18. Reyes, P.J.D.; Bornas, M.A.V.; Dominey-Howes, D.; Pidlaoan, A.C.; Magill, C.R.; Solidu, R.U., Jr. A synthesis and review of historical eruptions at Taal Volcano, Southern Luzon, Philippines. *Earth-Sci. Rev.* **2018**, *177*, 565–588. [CrossRef]
19. Vitale, S.; Isaia, R.; Ciarcia, S.; Di Giuseppe, M.G.; Iannuzzi, E.; Prinzi, E.P.; Tramparulo, F.D.A.; Troiano, A. Seismically induced soft-sediment deformation phenomena during the volcano-tectonic activity of Campi Flegrei caldera (southern Italy) in the last 15 kyr. *Tectonics* **2019**, *38*, 1999–2018. [CrossRef]
20. Acocella, V. Bridging the gap from caldera unrest to resurgence. *Front. Earth Sci.* **2019**, *7*, 173. [CrossRef]
21. Rosi, M.; Sbrana, A. Phlegrean fields. *Quad. Ric. Sci.* **1987**, *9*, 171.
22. Deino, A.L.; Orsi, G.; Piochi, M.; de Vita, S. The age of the Neapolitan Yellow Tuff caldera-forming eruption (Campi Flegrei caldera–Italy) assessed by 40Ar/39Ar dating method. *J. Volcanol. Geotherm. Res.* **2004**, *133*, 157–170. [CrossRef]
23. Giaccio, B.; Hajdas, I.; Isaia, R.; Deino, A.; Nomade, S. High-Precision 14C and 40Ar/39Ar Dating of the Campanian Ignimbrite (Y-5) Reconciles the Time-Scales of Climatic-Cultural Processes at 40 Kyr BP. *Sci. Rep.* **2017**, *7*, 45940. [CrossRef] [PubMed]

24. Di Vito, M.A.; Isaia, R.; Orsi, G.; Southon, J.; de Vita, S.; D'Antonio, M.; Pappalardo, L.; Piochi, M. Volcanism and deformation in the past 12 ka at the Campi Flegrei caldera (Italy). *J. Volcanol. Geotherm. Res.* **1999**, *91*, 221–246. [CrossRef]
25. Vitale, S.; Ciarcia, S. Tectono-stratigraphic setting of the Campania region (Southern Italy). *J. Maps* **2018**, *14*, 9–21. [CrossRef]
26. Vitale, S.; Prinzi, E.P.; Tramparulo, F.D.A.; De Paola, C.; Di Maio, R.; Piegari, E.; Sabbatino, M.; Natale, J.; Notaro, P.; Ciarcia, S. Late Miocene-early Pliocene out-of-sequence thrusting in the southern Apennines (Italy). *Geosciences* **2020**, *10*, 301. [CrossRef]
27. Isaia, R.; Vitale, S.; Di Giuseppe, M.G.; Iannuzzi, E.; Tramparulo, F.D.A.; Troiano, A. Stratigraphy, structure, and volcano-tectonic evolution of Solfatara maar-diatreme (Campi Flegrei, Italy). *Geol. Soc. Am. Bull.* **2015**, *127*, 1485–1504. [CrossRef]
28. Isaia, R.; Vitale, S.; Marturano, A.; Aiello, G.; Barra, D.; Ciarcia, S.; Iannuzzi, E.; Tramparulo, F.D.A. High-resolution geological investigations to reconstruct the long-term ground movements in the last 15 kyr at Campi Flegrei caldera (southern Italy). *J. Volcanol. Geotherm. Res.* **2019**, *385*, 143–158. [CrossRef]
29. Santacroce, R. Somma-Vesuvius. *Quad. Ric. Sci.* **1987**, *8*, 230.
30. Tramparulo, F.D.A.; Vitale, S.; Isaia, R.; Tadini, A.; Bisson, M.; Prinzi, E.P. Relation between alternating open/closed-conduit conditions and deformation patterns: An example from the Somma-Vesuvius volcano (southern Italy). *J. Struct. Geol.* **2018**, *112*, 138–153. [CrossRef]
31. Sbrana, A.; Marianelli, P.; Pasquini, G. Volcanology of Ischia (Italy). *J. Maps* **2018**, *14*, 494–503. [CrossRef]
32. Pappalardo, L.; Civetta, L.; D'Antonio, M.; Deino, A.; Di Vito, M.; Orsi, G.; Carandente, A.; De Vita, S.; Isaia, R.; Piochi, M. Chemical and Sr-isotopic evolution of the Phlegrean magmatic system before the Campanian Ignimbrite and the Neapolitan Yellow Tuff eruptions. *J. Volcanol. Geotherm. Res.* **1999**, *91*, 141–166. [CrossRef]
33. Scarpati, C.; Perrotta, A.; Lepore, S.; Calvert, A. Eruptive history of Neapolitan volcanoes: Constraints from 40Ar-39Ar dating. *Geol. Mag.* **2013**, *150*, 412–425. [CrossRef]
34. Orsi, G.; De Vita, S.; Di Vito, M. The restless, resurgent Campi Flegrei nested caldera (Italy): Constraints on its evolution andu configuration. *J. Volcanol. Geotherm. Res.* **1996**, *74*, 179–214. [CrossRef]
35. Silleni, A.; Giordano, G.; Isaia, R.; Ort, M.H. The magnitude of the 39.8 ka campanian ignimbrite eruption, Italy: Method, uncertainties and errors. *Front. Earth Sci.* **2020**, *8*, 543399. [CrossRef]
36. Acocella, V. Activating and reactivating pairs of nested collapses during caldera-forming eruptions: Campi Flegrei (Italy). *Geophys. Res. Lett.* **2008**, *35*, L17304. [CrossRef]
37. Vitale, S.; Isaia, R. Fractures and faults in volcanic rocks (Campi Flegrei, southern Italy): Insight into volcano-tectonic processes. *Int. J. Earth Sci.* **2014**, *103*, 801–819. [CrossRef]
38. Petrosino, P.; Arienzo, I.; Mazzeo, F.C.; Natale, J.; Petrelli, M.; Milia, A.; Perugini, D.; D'Antonio, M. The San Gregorio Magno lacustrine basin (Campania, southern Italy): Improved characterization of the tephrostratigraphic markers based on trace elements and isotopic data. *J. Quat. Sci.* **2019**, *34*, 393–404. [CrossRef]
39. Orsi, G.; Civetta, L.; Del Gaudio, C.; De Vita, S.; Di Vito, M.A.; Isaia, R.; Petrazzuoli, S.M.; Ricciardi, G.P.; Ricco, C. Short-term ground deformations and seismicity in the nested Campi Flegrei caldera (Italy). *J. Volcanol. Geotherm. Res.* **1999**, *91*, 415–451. [CrossRef]
40. Bevilacqua, A.; Isaia, R.; Neri, A.; Vitale, S.; Aspinall, W.P.; Bisson, M.; Bisson, M.; Flandoli, F.; Baxter, P.J.; Bertagnini, A.; et al. Quantifying volcanic hazard at Campi Flegrei caldera (Italy) with uncertainty assessment: I. Vent opening maps. *J. Geophys. Res.-Solid Earth* **2015**, *120*, 2309–2329. [CrossRef]
41. Bevilacqua, A.; Neri, A.; Bisson, M.; Esposti Ongaro, T.; Flandoli, F.; Isaia, R.; Rosi, M.; Vitale, S. The effects of vent location, event scale and time forecasts on pyroclastic density current hazard maps at Campi Flegrei caldera (Italy). *Front. Earth Sci.* **2017**, *5*, 72. [CrossRef]
42. Smith, V.C.; Isaia, R.; Pearce, N.J.C. Tephrostratigraphy and glass compositions of post-15 kyr Campi Flegrei eruptions: Implications for eruption history and chronostratigraphic markers. *Quat. Sci. Rev.* **2011**, *30*, 3638–3660. [CrossRef]
43. Bevilacqua, A.; Flandoli, F.; Neri, A.; Isaia, R.; Vitale, S. Temporal models for the episodic volcanism of Campi Flegrei caldera (Italy) with uncertainty quantification. *J. Geophys. Res.-Solid Earth* **2016**, *121*, 7821–7845. [CrossRef]
44. Isaia, R.; Marianelli, P.; Sbrana, A. Caldera unrest prior to intense volcanism in Campi Flegrei (Italy) at 4.0 ka B.P.: Implications for caldera dynamics and future eruptive scenarios. *Geophys. Res. Lett.* **2009**, *36*, L21303. [CrossRef]
45. Bevilacqua, A.; Neri, A.; De Martino, P.; Isaia, R.; Novellino, A.; Tramparulo, F.D.A.; Vitale, S. Radial interpolation of GPS and leveling data of ground deformation in a resurgent caldera: Application to Campi Flegrei (Italy). *J. Geod.* **2020**, *94*, 24. [CrossRef]
46. Sacchi, M.; Caccavale, M.; Corradino, M.; Esposito, G.; Ferranti, L.; Hámori, Z.; Horvath, F.; Insinga, D.; Marino, C.; Matano, F.; et al. The use and beauty of ultra-high-Resolution seismic reflection imaging in Late Quaternary marine volcaniclastic settings, Napoli Bay, Italy. *Földt. Közlöny* **2019**, *149*, 371. [CrossRef]
47. Natale, J.; Ferranti, L.; Isaia, R.; Marino, C.; Sacchi, M.; Spiess, V.; Steinmann, L.; Vitale, S. Integrated on-land-offshore stratigraphy of the Campi Flegrei caldera: New insights into the volcano-tectonic evolution in the last 15 kyr. *Basin Res.* **2022**, *34*, 855–882. [CrossRef]
48. Natale, J.; Ferranti, L.; Marino, C.; Sacchi, M. Resurgent dome faults in the offshore of the Campi Flegrei caldera (Pozzuoli Bay, Campania): Preliminary results from high-resolution seismic reflection profiles. *Boll. Geofis. Teor. Ed. Appl.* **2020**, *61*, 333–342.
49. Lambeck, K.; Antonioli, F.; Anzidei, M.; Ferranti, L.; Leoni, G.; Scicchitano, G.; Silenzi, S. Sea level change along the Italian coast during the Holocene and projections for the future. *Quat. Int.* **2011**, *232*, 250–257. [CrossRef]

50. Guidoboni, E.; Ciuccarelli, C. The Campi Flegrei caldera: Historical revision and new data on seismic crises, bradyseisms, the Monte Nuovo eruption and ensuing earthquakes (twelfth century 1582 ad). *Bull. Volcanol.* **2011**, *73*, 655–677. [CrossRef]
51. INGV. Monitoring Bullettin. 2022. Available online: https://www.ov.ingv.it (accessed on 1 June 2022).
52. Troiano, A.; Isaia, R.; Di Giuseppe, M.G.; Tramparulo, F.D.A.; Vitale, S. Deep Electrical Resistivity Tomography for a 3D picture of the most active sector of Campi Flegrei caldera. *Sci. Rep.* **2019**, *9*, 15124. [CrossRef]
53. Tamburello, G.; Caliro, S.; Chiodini, G.; De Martino, P.; Avino, R.; Minopoli, C.; Carandente, A.; Rouwet, D.; Aiuppa, A.; Costa, A.; et al. Escalating CO_2 degassing at the Pisciarelli fumarolic system, and implications for the ongoing Campi Flegrei unrest. *J. Volcanol. Geotherm. Res.* **2019**, *384*, 151–157. [CrossRef]
54. Isaia, R.; Di Giuseppe, M.G.; Natale, J.; Troiano, A.; Tramparulo, F.D.A.; Vitale, S. Volcano-tectonic setting of the Pisciarelli Fumarole Field, Campi Flegrei caldera, southern Italy: Insights into fluid circulation patterns and hazard scenarios. *Tectonics* **2021**, *40*, e2020TC006227. [CrossRef]
55. Folk, R.L.; Ward, W.C. Brazos River bar, a study in the significance of grain size parameters. *J. Sediment. Petrol.* **1957**, *27*, 3–26. [CrossRef]
56. Blair, T.C.; McPherson, J.G. Grain-size and textural classification of coarse sedimentary particles. *J. Sediment. Res.* **1999**, *69*, 6–19. [CrossRef]
57. Isaia, R.; D'Antonio, M.; Dell'Erba, F.; Di Vito, M.; Orsi, G. The Astroni volcano: The only example of closely spaced eruptions in the same vent area during the recent history of the Campi Flegrei caldera (Italy). *J. Volcanol. Geotherm. Res.* **2004**, *133*, 171–192. [CrossRef]
58. Camanni, G.; Roche, V.; Childs, C.; Manzocchi, T.; Walsh, J.; Conneally, J.; Delogkos, E. The three-dimensional geometry of relay zones within segmented normal faults. *J. Struct. Geol.* **2019**, *129*, 103895. [CrossRef]
59. Rodríguez-Pascua, M.A.; Silva, P.G.; Perez-Lopez, R.; Giner-Robles, J.L.; Martín-Gonzalez, F.; Del Moral, B. Polygenetic sand volcanoes: On the features of liquefaction processes generated by a single event (2012 Emilia Romagna 5.9 Mw earthquake, Italy). *Quat. Int.* **2015**, *357*, 329–335. [CrossRef]
60. De Vita, S.; Orsi, G.; Civetta, L.; Carandente, A.; D'Antonio, M.; Deino, A.; di Cesare, T.; Di Vito, M.A.; Fisher, R.V.; Isaia, R.; et al. The Agnano-Monte Spina eruption (4100 years BP) in the restless Campi Flegrei caldera (Italy). *J. Volcanol. Geotherm. Res.* **1999**, *91*, 269–301. [CrossRef]
61. Bartlett, S.F.; Youd, T.L. Empirical Analysis of Horizontal Ground Displacement Generated by Liquefaction-Induced Lateral Spread. Ph.D. Dissertation, Brigham Young University, Provo, UT, USA, 1992.
62. Araujo, W.; Ledezma, C. Factors That Affect Liquefaction-Induced Lateral Spreading in Large Subduction Earthquakes. *Appl. Sci.* **2020**, *10*, 6503. [CrossRef]
63. Makris, S.; Manzella, I.; Cole, P.; Roverato, M. Grain size distribution and sedimentology in volcanic mass-wasting flows: Implications for propagation and mobility. *Int. J. Earth Sci.* **2020**, *109*, 2679–2695. [CrossRef]
64. Rodríguez-Pascua, M.A.; Garduño-Monroy, V.H.; Israde-Alcantara, I.; Perez-Lopez, R. Estimation of the paleoepicentral area from the spatial gradient of deformationin lacustrine seismites (Tierras Blancas Basin, Mexico). *Quat. Int.* **2010**, *219*, 66–78. [CrossRef]
65. Fontana, D.; Amoroso, S.; Minarelli, L.; Stefani, M. Sand liquefaction induced by a blast test: New insights on source layer and grainsize segregation mechanisms (late Quaternary, Emilia, Italy). *J. Sediment. Res.* **2019**, *89*, 13–27. [CrossRef]
66. Diggs, T.N. An outcrop study of clastic injection structures in the Carboniferous Tesnus Formation, Marathon Basin, Trans-Pecos Texas. In *Sand Injectites: Implications for Hydrocarbon Exploration and Production*; Hurst, A., Cartwright, J., Eds.; AAPG: Tulsa, OK, USA, 2007; Volume 87, pp. 37–48.
67. Ross, J.A.; Peakall, J.; Keevil, G.M. An integrated model of extrusive sand injectites in cohesionless sediments. *Sedimentology* **2011**, *58*, 1693–1715. [CrossRef]